IOP PUBLISHING INVERSE PROBLEMS

Inverse Problems **23** (2007) 2311–2324 doi:10.1088/0266-5611/23/6/002

Numerical reconstruction of a cluster of small elastic inclusions

Hyeonbae Kang[1], **Eunjoo Kim**[1] **and June-Yub Lee**[2]

[1] Department of Mathematical Sciences and RIM, Seoul National University, Seoul 151-747, Korea
[2] Department of Mathematics, Ewha Womans University, Seoul 120-750, Korea

E-mail: hbkang@snu.ac.kr, kej@math.snu.ac.kr and jyllee@ewha.ac.kr

Received 8 June 2007, in final form 16 August 2007
Published 28 September 2007
Online at stacks.iop.org/IP/23/2311

Abstract

We consider a problem of reconstructing a cluster of small elastic inclusions which are located close to each other. We show that the location of the cluster and the elastic moment tensor associated with it can be reconstructed by the measurements of the displacement vectors on the boundary corresponding to the traction applied on the boundary. The detected elastic moment tensor represents the overall (or effective) property of the cluster of inclusions. We implement this idea of reconstruction for the two-dimensional linear isotropic elasticity to demonstrate its viability. We also perform a numerical study on the relation between the elastic moment tensor and the total size of the inclusions of general shape.

1. Introduction

Let Ω be an elastic body in $\mathbb{R}^d$ $(d = 2, 3)$ and suppose that multiple inclusions, which are close to each other (but not touching), are included in Ω. We consider the inverse problem of reconstructing the inclusions by means of a finite number of measurements of traction displacement on the boundary of Ω. Since the inclusions are closely spaced, it is unlikely that we will be able to reconstruct the individual inclusion separately with good resolution. Separating closely spaced inclusions requires very high-frequency information and the inverse problem under consideration is nonlinear and ill-posed. Thus it is natural to ask what kind of information of the cluster of inclusions we can detect from the boundary measurements.

In [7], Ammari *et al* considered an analogous problem to find a cluster of small conductive inclusions. They showed that the polarization tensor (and the location) associated with the cluster can be detected approximately by means of boundary measurements, and then showed that the polarization tensor yields an equivalent ellipse of the cluster. This equivalent ellipse represents the overall or effective property of the cluster as a conductor. In this paper, we adapt the same idea to detect a cluster of small elastic inclusions by means of boundary measurements

of the displacements. We will show that the location and the elastic moment tensor (EMT), which is a concept for elasticity analogous to the polarization tensor for electromagnetism, of the cluster can be found approximately and it represents the overall property of the cluster. We also perform some numerical experiments on the size estimates of the inclusions (not necessarily small) of general shape in terms of certain entries of the associated EMT.

There have been many efforts to detect electric or elastic inclusions using asymptotic expansions of the perturbation of the voltage or displacement on the boundary as the diameter of the inclusion tends to zero [7, 8, 11, 13, 14, 16, 18–20]. For a comprehensive study on the development in this direction, we refer to recent texts [5, 6]. We particularly mention that in [11] a MUSIC-type algorithm based on the asymptotic expansion formula was designed and implemented to reconstruct well-separated small electric inclusions. It would be interesting to combine the method in [11] and that of [7] (and this paper) to reconstruct well-separated clusters of electric (and elastic) inclusions. There also have been several significant works for the estimation of the total size of inclusions [1–4, 12, 21].

This paper is organized as follows. In section 2, we define the EMT associated with multiple inclusions and some of its important properties are explained. In section 3, we derive an asymptotic expansion formula for the displacement perturbation in the presence of a cluster of small inclusions and then explain the reconstruction algorithm based on the asymptotic formula. Since derivation of the properties of the EMT for multiple inclusions and asymptotic expansion is similar to those in [7, 8, 19], we will be brief. The details of the derivation of the properties of the EMT for multiple inclusions can be found in [17]. The last section presents the results of numerical experiments.

2. Layer potentials for the Lamé system

Let Ω be a bounded Lipschitz domain in $\mathbb{R}^d$, $d = 2, 3$, which occupies a homogenous isotropic elastic body with the Lamé constants (λ, μ) satisfying $\mu > 0$ and $d\lambda + 2\mu > 0$, so that the elasticity tensor $C = (C_{ijkl})$ for Ω is given by

$$C_{ijkl} = \lambda\delta_{ij}\delta_{kl} + \mu(\delta_{ik}\delta_{jl} + \delta_{il}\delta_{jk}), \qquad i, j, k, l = 1, \ldots, d. \tag{2.1}$$

For a given displacement vector $\mathbf{u}$, the strain is defined to be

$$\mathcal{E}(\mathbf{u}) := \tfrac{1}{2}(\nabla\mathbf{u} + \nabla\mathbf{u}^{\mathrm{T}}), \tag{2.2}$$

where T denotes the transpose. The elastostatic system corresponding to C is defined by

$$\mathcal{L}_{\lambda,\mu}\mathbf{u} := \nabla \cdot (C\mathcal{E}(\mathbf{u})) = \mu\triangle\mathbf{u} + (\lambda + \mu)\nabla(\nabla \cdot \mathbf{u}), \tag{2.3}$$

and the corresponding conormal derivative $\frac{\partial \mathbf{u}}{\partial \nu}$ on the boundary $\partial\Omega$ is defined to be

$$\frac{\partial \mathbf{u}}{\partial \nu} := C\mathcal{E}(\mathbf{u})N = \lambda(\nabla \cdot \mathbf{u})N + \mu(\nabla\mathbf{u} + \nabla\mathbf{u}^{\mathrm{T}})N, \tag{2.4}$$

where N is the outward unit normal to $\partial\Omega$.

The Kelvin matrix of fundamental solutions $\Gamma = (\Gamma_{ij})_{i,j=1}^{d}$ for $\mathcal{L}_{\lambda,\mu}$ is defined by

$$\Gamma_{ij}(x) := \begin{cases} -\dfrac{\gamma_1}{4\pi}\dfrac{\delta_{ij}}{|x|} - \dfrac{\gamma_2}{4\pi}\dfrac{x_i x_j}{|x|^3}, & \text{if} \quad d = 3, \\ \dfrac{\gamma_1}{2\pi}\delta_{ij}\log|x| - \dfrac{\gamma_2}{2\pi}\dfrac{x_i x_j}{|x|^2}, & \text{if} \quad d = 2, \end{cases} \tag{2.5}$$

where

$$\gamma_1 = \frac{1}{2}\left(\frac{1}{\mu} + \frac{1}{2\mu + \lambda}\right) \qquad \text{and} \qquad \gamma_2 = \frac{1}{2}\left(\frac{1}{\mu} - \frac{1}{2\mu + \lambda}\right).$$

The single- and double-layer potential of the density function $\phi \in L^2(\partial\Omega)^d$ associated with the Lamé parameters (λ, μ) are defined by

$$\mathcal{S}_\Omega[\phi](x) := \int_{\partial\Omega} \Gamma(\mathbf{x}-\mathbf{y})\phi(y)\,d\sigma(y), \qquad x \in \mathbb{R}^d, \tag{2.6}$$

$$\mathcal{D}_\Omega[\phi](x) := \int_{\partial\Omega} \frac{\partial}{\partial \nu_y}\Gamma(\mathbf{x}-\mathbf{y})\phi(y)\,d\sigma(y), \qquad x \in \mathbb{R}^d\backslash\partial\Omega, \tag{2.7}$$

where $\frac{\partial}{\partial \nu_y}$ denotes the conormal derivative defined in (2.4) with respect to y-variables.

We now define the EMT associated with multiple inclusions. Let D_s, $s = 1, \dots, m$, be a bounded Lipschitz simply connected domain whose closures are mutually disjoint. Suppose that the Lamé parameters of D_s are (λ_s, μ_s) for $s = 1, \dots, m$. Let $D := \cup_{s=1}^m D_s$. Let (λ, μ) be the Lamé parameters of the background matrix so that the elasticity tensor in this case is given by

$$C_{ijkl} = \left\{\lambda\chi(\mathbb{R}^d\backslash D) + \sum_{s=1}^m \lambda_s \chi(D_s)\right\}\delta_{ij}\delta_{kl} + \left\{\mu\chi(\mathbb{R}^d\backslash D) + \sum_{s=1}^m \mu_s\chi(D_s)\right\}(\delta_{ik}\delta_{jl} + \delta_{il}\delta_{jk}).$$

It is assumed that $\mu_s > 0$ and $d\lambda_s + 2\mu_s > 0$ for $s = 1, \dots, m$. For a given function $\mathbf{h}$ satisfying $\mathcal{L}_{\lambda,\mu}\mathbf{h} = 0$ in $\mathbb{R}^d$, consider the following elastostatic system in $\mathbb{R}^d$:

$$\begin{cases} \nabla\cdot(C\mathcal{E}(\mathbf{u})) = 0, & \text{in} \quad \mathbb{R}^d, \\ \mathbf{u}(x) - \mathbf{h}(x) = O(|x|^{1-d}) & \text{as} \quad |x| \to \infty. \end{cases} \tag{2.8}$$

One can easily see that (2.8) is equivalent to the following problem:

$$\begin{cases} \mathcal{L}_{\lambda,\mu}\mathbf{u} = 0 & \text{in} \quad \mathbb{R}^d\backslash\overline{D}, \\ \mathcal{L}_{\lambda_s,\mu_s}\mathbf{u} = 0 & \text{in} \quad D_s, \quad s = 1, \dots, m, \\ \mathbf{u}|_+ = \mathbf{u}|_- & \text{on} \quad \partial D_s, \quad s = 1, \dots, m, \\ \left.\dfrac{\partial \mathbf{u}}{\partial \nu}\right|_+ = \left.\dfrac{\partial \mathbf{u}}{\partial \nu_s}\right|_- & \text{on} \quad \partial D_s, \quad s = 1, \dots, m, \\ \mathbf{u}(x) - \mathbf{h}(x) = O(|x|^{1-d}) & \text{as} \quad |x| \to \infty, \end{cases} \tag{2.9}$$

where $\mathcal{L}_{\lambda_s,\mu_s}$ and $\frac{\partial}{\partial \nu_s}$ denote, respectively, the Lamé system and the conormal derivative with respect to the parameter (λ_s, μ_s).

In view of the transmission conditions (the third and fourth equations in (2.9)) along ∂D_s, it is natural to represent the solution $\mathbf{u}$ to (2.8) using the single-layer potentials. For $s = 1, \dots, m$, let $\mathcal{S}^s_{D_s}[\phi]$ be the single-layer potential on ∂D_s defined using the Lamé parameters (λ_s, μ_s). Then the solution $\mathbf{u}$ of (2.9) can be represented as

$$\mathbf{u}(x) = \begin{cases} \mathbf{h}(x) + \sum_{s=1}^m \mathcal{S}_{D_s}[\mathbf{g}_s](x), & x \in \mathbb{R}^d \setminus \bar{D}, \\ \mathcal{S}^s_{D_s}[\mathbf{f}_s](x), & x \in D_s, \quad s = 1, \dots, m, \end{cases} \tag{2.10}$$

where $(\mathbf{f}_1, \dots, \mathbf{f}_m, \mathbf{g}_1, \dots, \mathbf{g}_m) \in L^2(\partial D_1)^d \times \cdots \times L^2(\partial D_m)^d \times L^2_\Psi(\partial D_1) \times L^2_\Psi(\partial D_m)$ is the unique solution to

$$\begin{cases} \mathcal{S}^s_{D_s}[\mathbf{f}_s] - \mathcal{S}_{D_s}[\mathbf{g}_s] - \sum_{t\neq s} \mathcal{S}_{D_t}[\mathbf{g}_t] = \mathbf{h}, \\ \left.\dfrac{\partial\left(\mathcal{S}^s_{D_s}[\mathbf{f}_s]\right)}{\partial \nu_s}\right|_- - \left.\dfrac{\partial\left(\mathcal{S}_{D_s}[\mathbf{g}_s]\right)}{\partial \nu}\right|_+ - \sum_{t\neq s}\left.\dfrac{\partial\left(\mathcal{S}_{D_t}[\mathbf{g}_t]\right)}{\partial \nu}\right|_{\partial D_s} = \dfrac{\partial \mathbf{h}}{\partial \nu}, \end{cases} \quad \text{on} \quad \partial D_s, \tag{2.11}$$

for $s = 1, \dots, m$. Here $L^2_\Psi(\partial D_s)$ is defined by

$$L^2_\Psi(\partial D_s) := \left\{ \mathbf{f} \in L^2(\partial D_s)^d \,\middle|\, \int_{\partial D_s} \mathbf{f} \cdot \psi \, d\sigma = 0 \right. \\ \left. \text{for all linear functions } \psi \text{ satisfying } \partial_i \psi_j + \partial_j \psi_i = 0,\ 1 \leqslant i, j \leqslant d \right\}.$$

Let us briefly explain the unique solvability of (2.11). Since $\overline{D}_s$ is mutually disjoint, $\mathcal{S}_{D_t}[f]$ is smooth in a neighborhood of ∂D_s for any $f \in L^2(\partial D_t)$ if $t \neq s$. Therefore, the system of integral equations (2.11) is a compact perturbation of the system

$$\begin{cases} \mathcal{S}^s_{D_s}[\mathbf{f}_s] - \mathcal{S}_{D_s}[\mathbf{g}_s] = \mathbf{h}, \\ \dfrac{\partial\left(\mathcal{S}^s_{D_s}[\mathbf{f}_s]\right)}{\partial \nu_s}\bigg|_- - \dfrac{\partial\left(\mathcal{S}_{D_s}[\mathbf{g}_s]\right)}{\partial \nu}\bigg|_+ = \dfrac{\partial \mathbf{h}}{\partial \nu}, \end{cases} \qquad \text{on} \quad \partial D_s, \quad s = 1, \dots, m. \tag{2.12}$$

It was proved in [15] that (2.12) is uniquely solvable for each s under the assumption that both $(\lambda - \lambda_s)$ and $(\mu - \mu_s)$ are either positive or negative. Thus to prove the solvability of (2.11) it suffices to show its injectivity by the Fredholm alternative, which can be proved in a way similar to that for the conductivity equation in [7]. A detailed proof of the solvability of (2.11) can be found in [17].

In particular, let $\mathbf{h}(x) = x_i \mathbf{e}_j$ where $\mathbf{e}_j$, $j = 1, \dots, d$, is the standard basis for $\mathbb{R}^d$. Let $\left(\mathbf{f}^{ij}_1, \dots, \mathbf{f}^{ij}_m, \mathbf{g}^{ij}_1, \dots, \mathbf{g}^{ij}_m\right)$ be the solution to (2.11) with $\mathbf{h} = x_i \mathbf{e}_j$. It then follows from (2.10) and the expansion

$$\Gamma(x - y) = \Gamma(x) + \sum_{k=1}^{d} \partial_k \Gamma(x) y_k + O(|x|^{-d}) \tag{2.13}$$

for y in a bounded set and $|x| \to \infty$ that the solution $\mathbf{u}$ to (2.9) with $\mathbf{h} = x_i \mathbf{e}_j$ satisfies

$$\mathbf{u}(x) = x_i \mathbf{e}_j + \sum_{p=1}^{d} \partial_p \Gamma(x) \sum_{s=1}^{m} \int_{\partial D_s} y_p \mathbf{g}^{ij}_s(y) \, d\sigma(y) + O(|x|^{-d}), \qquad |x| \to \infty. \tag{2.14}$$

The EMT for the multiple inclusion $D = \cup_{s=1}^m D_s$ is defined by

$$M^{ij}_{pq} = \sum_{s=1}^{m} \int_{\partial D_s} (x_p \mathbf{e}_q) \cdot \mathbf{g}^{ij}_s \, d\sigma, \qquad i, j, p, q = 1, \dots, d. \tag{2.15}$$

Using the EMT, (2.14) takes the form

$$u_k(x) = x_i \delta_{jk} + \sum_{p,q=1}^{d} \partial_p \Gamma_{kq}(x) M^{ij}_{pq} + O(|x|^{-d}), \qquad k = 1, \dots, d, \tag{2.16}$$

where u_k is the kth component of $\mathbf{u}$. In other words, the first-order term of the perturbation of the displacement vector observed at ∞ is completely determined by the EMT.

The following theorem is obtained in [17] using arguments similar to those in [7].

Theorem 2.1.

(i) (Symmetry) For $p, q, i, j = 1, \dots, d$, the following hold:

$$M^{ij}_{pq} = M^{ij}_{qp}, \qquad M^{ij}_{pq} = M^{ji}_{pq} \qquad \text{and} \qquad M^{ij}_{pq} = M^{pq}_{ij}. \tag{2.17}$$

(ii) (Positivity) Suppose that all the Lamé parameters of the inclusions are the same, i.e., $\lambda_s = \widetilde{\lambda}$ *and* $\mu_s = \widetilde{\mu}$ *for all* $s = 1, \ldots, m$. *If* $\mu > \tilde{\mu}$ *and* $\lambda > \widetilde{\lambda}$ ($\mu < \tilde{\mu}, \lambda < \widetilde{\lambda}$), *then* M *is positive (negative, resp.) definite on the space of symmetric matrices. Let* κ *be an eigenvalue of* M. *Then there are constants* C_1 *and* C_2 *depending on* $\lambda, \mu, \tilde{\lambda}, \tilde{\mu}$ *such that*

$$C_1|D| \leqslant |\kappa| \leqslant C_2|D|. \tag{2.18}$$

(iii) (Size estimation) Suppose $i \neq j$. *Under the same condition as (ii), there exists a constant* C *depending on* $\lambda, \mu, \tilde{\lambda}, \tilde{\mu}$ *such that*

$$\mu \left| \frac{\mu + \tilde{\mu}}{\mu - \tilde{\mu}} \right| |D| \leqslant \left| M_{ij}^{ij} \right| \leqslant C|D|. \tag{2.19}$$

3. Asymptotic expansions and the reconstruction algorithm

We now briefly explain the asymptotic expansion of the displacement perturbation due to the presence of a cluster of small inclusions. Let D denote the (single) cluster of inclusions contained in an elastic body Ω. More precisely, D can be modeled as $D = \epsilon\left(\cup_{s=1}^m B_s\right) + z$, where B_s are mutually disjoint bounded domains such that the volume of $\cup_{s=1}^m B_s$ is 1 and the center of mass of $\cup_{s=1}^m B_s$ is the origin, ϵ is small and represents the order of magnitude of the inclusion D and z represents the location of the inclusion. If we put $D_s = \epsilon B_s$, $s = 1, \ldots, m$, then the distance among D_s is of order ϵ and hence D represents a collection of closely spaced multiple small inclusions. We suppose that each D_s is an isotropic elastic material with the Lamé parameters (μ_s, λ_s) and the background $D_0 := \Omega \backslash D$ is also isotropic with different Lamé parameters μ and λ. So the elasticity tensor of $C = (C_{ijkl})$ of Ω is given by

$$C_{ijkl} = \left\{ \lambda \chi(\Omega \backslash D) + \sum_{s=1}^m \lambda_s \chi(D_s) \right\} \delta_{ij}\delta_{kl} + \left\{ \mu \chi(\Omega \backslash D) + \sum_{s=1}^m \mu_s \chi(D_s) \right\} (\delta_{ik}\delta_{jl} + \delta_{il}\delta_{jk}),$$

This paper is concerned with reconstruction of the inclusions D by means of measurements of the displacement occurred by the traction applied on the boundary of Ω. Mathematically, the displacement vector $\mathbf{u}$ is the solution to the problem

$$\begin{cases} \nabla \cdot (C\mathcal{E}(\mathbf{u})) = 0 & \text{in} \quad \Omega, \\ \dfrac{\partial \mathbf{u}}{\partial \nu} = \mathbf{g} & \text{on} \quad \partial\Omega, \end{cases} \tag{3.1}$$

where $\mathbf{g}$ represents the traction on $\partial\Omega$. The measurement for the reconstruction is $\mathbf{u}|_{\partial\Omega}$, which is the displacement on $\partial\Omega$.

Note that since the inclusions D_s are very closely located, it is unlikely that the individual inclusion can be reconstructed. However, as we will see in the following section, we can reconstruct an ellipse which represents the cluster of inclusions (and the Lamé parameters) as a whole. This ellipse is called an *equivalent ellipse* and is approximately an effective property of the cluster of inclusions as an elastic body.

The algorithm for the reconstruction is based on the asymptotic expansion of the perturbation of the displacement which can be derived in a way which is almost parallel to that in [19]. So, we simply mention the formula without the detail of derivation. The algorithm itself is identical to that in [19], so we refer the reader to that paper.

For a given traction $\mathbf{g}$, let $\mathbf{u}$ be the solution of the problem (3.1). Define the function $\mathbf{H}[\mathbf{g}]$ by

$$\mathbf{H}[\mathbf{g}](x) = -\mathcal{S}_\Omega[\mathbf{g}](x) + \mathcal{D}_\Omega[\mathbf{u}|_{\partial\Omega}](x), \qquad x \in \mathbb{R}^d \backslash \partial\Omega. \tag{3.2}$$

The following asymptotic formula for $\mathbf{H}[\mathbf{g}]$ can be obtained in the same manner as in [19].

Theorem 3.1. *Let $H_k[\mathbf{g}]$, $k = 1, \ldots, d$, be the component of* $\mathbf{H}[\mathbf{g}]$. *For $x \in \mathbb{R}^d \backslash \overline{\Omega}$,*

$$H_k[\mathbf{g}](x) = \epsilon^d \sum_{i,j,p,q=1}^{d} (\partial_i U_j)(z) \partial_p \Gamma_{kq}(x - z) M_{pq}^{ij} + O\left(\frac{\epsilon^d}{|x|^d}\right) + O\left(\frac{\epsilon^{d+1}}{|x|^{d-1}}\right), \quad |x| \to \infty, \tag{3.3}$$

where $\mathbf{U} = (U_1, \ldots, U_d)$ is the solution to the Lamé system without the inclusion, i.e., the solution to

$$\begin{cases} \nabla \cdot (C^0 \mathcal{E}(\mathbf{u})) = 0 & \text{in} \quad \Omega, \\ \dfrac{\partial \mathbf{u}}{\partial \nu} = \mathbf{g} & \text{on} \quad \partial\Omega, \end{cases} \tag{3.4}$$

with $C_{ijkl}^0 = \lambda \delta_{ij} \delta_{kl} + \mu(\delta_{ik}\delta_{jl} + \delta_{il}\delta_{jk})$, M_{pq}^{ij} are the elastic moment tensors associated with $\cup_{s=1}^m B_s$ and Γ is the Kelvin matrix of fundamental solutions corresponding to the Lamé parameters (λ, μ).

Observe that the function $\mathbf{H}[\mathbf{g}]$ can be computed using the boundary measurement $\mathbf{u}|_{\partial\Omega}$. Formula (3.3) says that $\mathbf{H}[\mathbf{g}](x)$ is approximately

$$\epsilon^d \sum_{i,j,p,q=1}^{d} (\partial_i U_j)(z) \partial_p \Gamma_{kq}(x - z) M_{pq}^{ij} \tag{3.5}$$

when $|x|$ is large. So we can recover the location z and the EMT $\epsilon^d M_{pq}^{ij}$ by $\mathbf{H}[\mathbf{g}](x)$. The equivalent ellipse, which represents the overall (or effective) property of the cluster of inclusions, can be computed from the detected EMT. The details of the reconstruction algorithm and computing the equivalent ellipse from the EMT can be found in [19].

4. Numerical experiments

In this section, we show some numerical experiments illustrating computational usability of the theoretical results in the previous sections. We developed a forward integral equation solver for the elastic inclusion problem (3.1) with multiple inclusions in the two-dimensional space. Our solver achieves fourth-order accuracy and provides about four digits of accuracy for the elastic moment tensor when each of inclusion interfaces has been discritized with $N = 256$ points.

We observe in the second example that M_{12}^{12} component of the EMT is proportional to the total size of inclusions and the proportional constant strongly depends on the Lamé constant $\tilde{\mu}$ when all inclusions have the same constant $\mu_s = \tilde{\mu}$. Example 3 further investigates the cases where the Lamé constants of inclusions are different from each other. If all inclusions have either larger or smaller μ_s than μ, it is easy to estimate the total inclusion size from the measurement M_{12}^{12}. However, M_{12}^{12} may be pretty small if some of inclusions are stiffer and some are softer than the background medium.

Example 4 shows the results of disc and ellipse reconstruction algorithms with the aid of a quadratic center finding method for inclusions with the same Lamé constant. The ellipse reconstruction algorithm requires the Lamé constants $\tilde{\mu}$ of inclusions and it gives better performance than the disc algorithm which is applicable without knowledge on the Lamé constants of the inclusions. The last example presents the results of reconstruction algorithms for a domain with inclusions having different Lamé constants. We developed a concept of μ-area, area of an inclusion weighted by a factor depending on μ, $D_s \frac{\mu - \mu_s}{\mu + \mu_s} |D_s|$ and show that the computed center is close to the geometric mean of centers of the inclusions weighted by

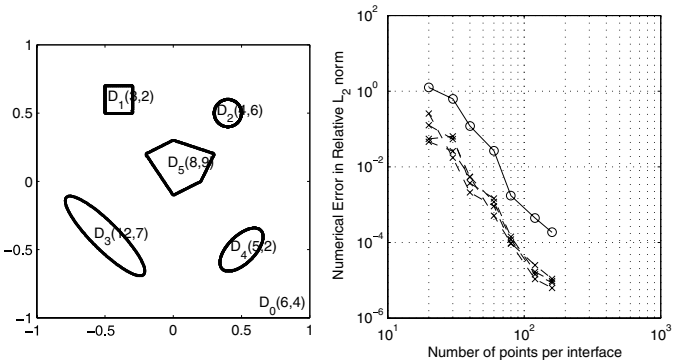

Figure 1. Convergence error of the forward solver with $N = 20$–160 for the domain with five inclusions D_s whose Lamé constants are (λ_s, μ_s). Four broken lines represent the convergence errors of $u^{1,1}$, $u^{1,2}$, $u^{2,2}$ and u^{quad}. The solid line does that of M^{ij}_{pq}.

the μ-area. Also we demonstrate that the concept of effective Lamé constant μ_* related to μ-area is useful for the disc and the ellipse reconstruction algorithm.

It is also worth remarking that these numerical experiments are generalization of our previous work [19] for the cases of multiple inclusions with different Lamé constants and the reconstruction algorithms for single and multiple inclusions show many similarities. Thus we do not repeat some of the interesting and important validation experiments in this paper; for example, the ellipse reconstruction algorithm is linearly stable with respect to random noise which was shown in the second example in [19].

Example 1 (convergence of a forward solver)**.** We implement an integral equation solver in order to generate forward solutions of the Neumann-type elastic inclusion problem (3.1). A generalized minimum residual (GMRES) method has been used to solve the system of integral equations (2.10)–(2.11) and the single- and double-layer potential defined in (2.6) and (2.7) have been numerically evaluated using the trapezoidal rule with equally spaced discretization points along the interfaces ∂D_s. The integrable singularities of the integral kernels (2.5) have been removed using a delta-trigonometric-type method [9] in order to achieve at least fourth-order accuracy. The procedure is implemented in Fortran for two-dimensional problems with multiple inclusions.

We demonstrate the convergence error of the forward solver using the four computed inhomogeneous solutions $u^{1,1}$, $u^{1,2}$, $u^{2,2}$ and u^{quad} which denote the inhomogeneous solutions with the same boundary values (traction) of the corresponding homogeneous solutions, $U^{1,1} = (2x, 0)$, $U^{1,2} = (y, x)$, $U^{2,2} = (0, y)$, $U^{\text{quad}} = (2xy, x^2 - y^2)$, respectively. There are five inclusions $D_1, \ldots, D_5$ with the various Lamé constants (λ_s, μ_s) for $s = 1, \ldots, 5$ while the background Lamé constant is fixed to $(\lambda, \mu) = (6, 4)$ as shown in the left diagram of figure 1. We compute coarse grid solutions with $N = 20$–160 equispaced points on each of the five interfaces ∂D_s and compare them with the corresponding forward solutions on the finer grid with $N = 480$. The four broken lines in the right diagram represent the convergence errors of $u^{1,1}$, $u^{1,2}$, $u^{2,2}$ and u^{quad} in the root-mean-square norm. The solid line with circles draws the convergence error of M^{ij}_{pq} in a component-wise l_2 sense. The numerical experiment shows that the forward integral equation solver achieves fourth-order convergence and provides about five digits of accuracy for the forward solutions and four digits for M^{ij}_{pq} when $N = 256$.

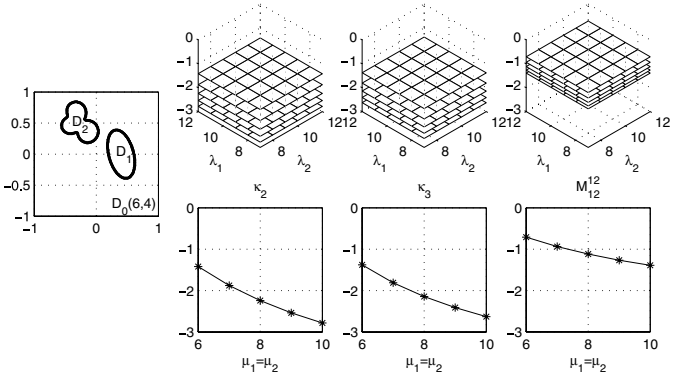

Figure 2. Eigenvalues κ_2, κ_3 and the elastic moment tensor M_{12}^{12} for the domain shown in the leftmost figure. The upper figures show κ_2, κ_3 and M_{12}^{12} as functions of λ_1, λ_2 with $\tilde{\mu} = 6, 7, 8, 9, 10$. The bottom plots show the same results as functions of $\tilde{\mu}$ with fixed $\lambda_1 = \lambda_2 = 10$.

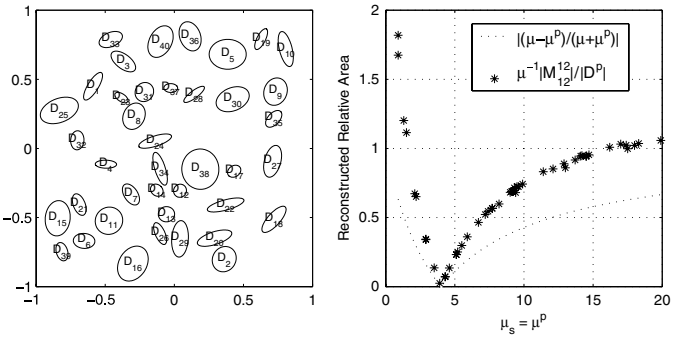

Figure 3. The reconstructed relative area as a function of μ^p and its theoretical lower bound $|\frac{\mu-\mu^p}{\mu+\mu^p}|$. The stars $(*)$ show the computed results $\frac{|M_{12}^{12}|}{\mu}$ relative to the inclusion size $|D^p|$.

Example 2 (EMT as a function of $\tilde{\lambda}$ and $\tilde{\mu}$)**.** The elastic moment tensor M defined in section 2 is symmetric (2.17) and its eigenvalues κ are bounded by the size of inclusions (theorem 2.1 (ii)). We numerically investigate how the components and the eigenvalues of the EMT depend on the Lamé constants of the inclusions.

We compute M_{12}^{12}, and the second and third eigenvalues κ_2, κ_3 of the EMT for the domain shown in figure 2 as a function of λ_s and μ_s while (λ, μ) are fixed as $(6, 4)$. The upper three plots show κ_2, κ_3 and M_{12}^{12} as functions of $7 \leqslant \lambda_1 \leqslant 12$ and $7 \leqslant \lambda_2 \leqslant 12$ for five different cases where $\mu_1 = \mu_2 = \tilde{\mu} = 6, 7, 8, 9, 10$. The lower three plots show the same values but in different view points, that is, as functions of $\tilde{\mu}$. It is easy to find that these three values are strongly dependent on $\tilde{\mu}$ but almost independent of λ_s.

The following numerical experiment demonstrates that M_{12}^{12} is a function of $\tilde{\mu}$ and the size of inclusions can be easily estimated from the elastic moment tensor M_{12}^{12} and $\tilde{\mu}$. We first select 50 random values for $0.5 \leqslant \lambda^p \leqslant 20$ and another 50 random values for $0.5 \leqslant \mu^p \leqslant 20$, $p = 1, \ldots, 50$. Then we choose up to 20 inclusions among 40 ellipses shown in figure 3 in order to generate a computation domain D^p for each $p = 1, \ldots, 50$ and set the same Lamé constants for all inclusions, $\lambda_s = \tilde{\lambda} = \lambda^p$ and $\mu_s = \tilde{\mu} = \mu^p$ for $D_s \subset D^p$ while

the background Lamé constants are fixed to $(\lambda, \mu) = (6, 4)$. The 50 star marks $*$ in figure 3 indicate the absolute values of $\frac{1}{\mu}|M_{12}^{12}|$ normalized with $|D^p|$. The numerical result shows that the estimated size $\frac{1}{\mu}|M_{12}^{12}|$ is only twice the theoretical lower bound $\left|\frac{\mu-\mu^p}{\mu+\mu^p}\right||D^p|$ which has been written in theorem 2.1 (iii). The estimated size is near zero if $\tilde{\mu}$ is pretty close to μ and it is larger than the actual size if $\tilde{\mu}$ is much smaller than or much larger than μ, say $\tilde{\mu} < \frac{1}{2}\mu$ or $4\mu < \tilde{\mu}$.

Example 3 (area reconstruction of multiple inclusions)**.** We observed in the previous example that the moment tensor $\frac{1}{\mu}|M_{12}^{12}|$ is proportional to the size of inclusions and the proportional constant is a function of $\frac{\mu-\tilde{\mu}}{\mu+\tilde{\mu}}$ when all inclusions have the same Lamé constants $\tilde{\mu}$. We now investigate domains in which inclusions of various shapes have different Lamé constants. Figure 4 shows three domains containing nine inclusions each and the reconstructed size $\frac{1}{\mu}|M_{12}^{12}|$. The first domain has nine inclusions which are stiffer than the background medium $\lambda_s > \lambda, \mu_s > \mu$, the second domain contains nine soft inclusions $\lambda_s < \lambda, \mu_s < \mu$. The third domain incorporates five stiff (marked by $\square$), three soft (marked by $\bigcirc$) inclusions and one inclusion with $\lambda_s \neq \lambda, \mu_s = \mu$.

For each of the three cases, we performed nine experiments for a domain with m-inclusions, $D^m := \cup_{s=1}^m D_s$. The dash-dotted lines with the stars $(*)$ in the rightmost figures show the actual size of the inclusions, $|D^m| = \sum_{s=1}^m |D_s|$. The solid lines plot the computed size $\frac{1}{\mu}|M_{12}^{12}|$ and the triangle marks on the solid lines indicate the sign of M_{12}^{12}, $\triangle$ for positive and ∇ for negative. The dotted lines are for the lower bounds of the estimated size $\left|\sum_{s=1}^L \frac{\mu-\tilde{\mu}}{\mu+\tilde{\mu}}|D_s|\right|$ and $\square$ or $\bigcirc$ marker indicates whether the mth inclusion is stiff or soft.

In the top plot in figure 4 where the inclusions are stiffer than the background medium, $(\mu = 4) < 6 \leqslant \mu_s \leqslant 12$, the reconstructed size is between the actual size and the lower bound. More precisely, it is about twice as large as the lower bound but just a little larger than half of the actual size, which can be easily guessed from figure 3 of the previous experimentation with $\tilde{\mu}$ around 5–10. The reconstructed size for the middle case where $1 \leqslant \mu_s \leqslant 8 < (\mu = 9)$ is pretty close to the actual size. It is sometimes bigger than the actual size; in particular it is more than double for the first experimentation with $D^1 = D_1$ and $\mu_1 = 1 \ll \mu = 9$.

The third case with mixed inclusion is little more complex than the previous cases. The first inclusion (marked by $\bigcirc$) is soft ($\mu_1 = 1$) compared to the background ($\mu = 4$), so the sign of M_{12}^{12} for D^1 is positive (marked by $\triangle$). The second inclusion, however, is stiff and its contribution to M_{12}^{12} is negative, thus the reconstruction size $\frac{1}{\mu}|M_{12}^{12}|$ is decreasing. We can define the concept of effective stiffness using the sign of M_{12}^{12}, then $D^1, \ldots, D^3$ contains effectively stiff inclusions and $D^4, \ldots, D^9$ does effectively soft inclusions. The effect of adding one more stiff inclusion to a domain with effectively soft inclusions is negative to the reconstructed size, as we can see for the cases $m = 2, m = 3$. Also the reconstructed size is also decreasing for the cases $m = 7, m = 9$ and no effect when $\mu_8 = \mu$. Therefore, the reconstructed size may be much smaller than the actual size if the effects of stiff and soft inclusions cancel each other as seen in the bottom case.

Example 4 (ellipse reconstruction algorithm)**.** In this example, we find a disc or an ellipse to reconstruct multiple inclusions with various shapes. The disc and ellipse reconstruction algorithms presented in [19] have been developed for the single inclusion case. However, the same algorithms work perfectly well for the cases of multiple inclusions.

The disc reconstruction simply estimates the size of inclusion as

$$|D_{\text{disc}}| = \frac{1}{\mu}|M_{12}^{12}|; \tag{4.1}$$

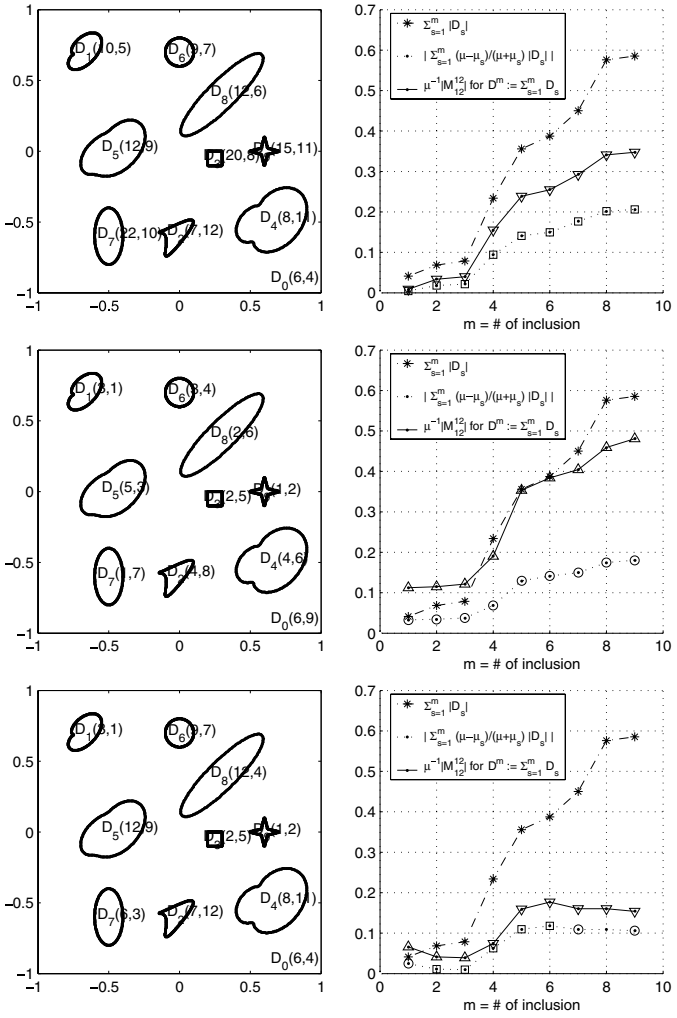

Figure 4. Geometric configurations with stiff(top), soft(middle), mixed(bottom) inclusions and estimated area. Dash-dotted lines with the stars $(*)$ are for actual sizes $|D^m := \cup_{i=s}^m D_s|$, solid lines for computed sizes $\frac{1}{\mu}|M_{12}^{12}|$ and dotted lines for the theoretical lower bounds $|\sum_{s=1}^m \frac{\mu-\tilde{\mu}}{\mu+\tilde{\mu}}|D_s||$. $\triangle(\nabla)$ marks on the solid lines indicate $+(-)$ sign of M_{12}^{12} for D^m and $\square(\bigcirc)$ marks on the dotted lines indicate stiff(soft) inclusion.

therefore, it can be applicable without prior knowledge of the Lamé constants of the inclusions. The ellipse reconstruction algorithm, which requires the estimated Lamé constants of the inclusions, first determines the angle of rotation θ by solving the following equation:

$$\frac{M_{12}^{11} + M_{22}^{12}}{M_{11}^{11} - M_{22}^{22}} = \frac{1}{2}\tan 2\theta, \qquad 0 \leqslant \theta < \frac{\pi}{2}.$$

Then the algorithm finds the size $|D_{\text{ellipse}}|$ and the EMT m of an ellipse which satisfy the following equations:

$$2\big(\hat{m}_{22}^{11} + 2\hat{m}_{12}^{12}\big) - \big(\hat{m}_{11}^{11} + \hat{m}_{22}^{22}\big) = 2\big(\hat{M}_{22}^{11} + 2\hat{M}_{12}^{12}\big) - \big(\hat{M}_{11}^{11} + \hat{M}_{22}^{22}\big), \qquad \hat{m}_{12}^{12} = \hat{M}_{12}^{12}, \quad (4.2)$$

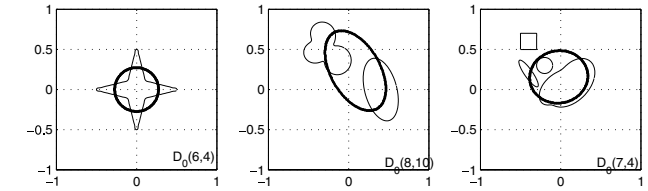

(λ, μ)	(λ_s, μ_s)	$\lvert D\rvert$	$\lvert D_{disk}\rvert$	$\lvert D_{ellipse}\rvert$	(x_c, y_c)
(6, 4)	(9, 6)	0.2346	0.0843	0.2345	(-0.0002, 0.0003)
(8, 10)	(3, 5)	0.4826	0.3990	0.5269	(0.0849, 0.2353)
(7, 4)	(12, 10)	0.3854	0.2823	0.3722	(-0.0238, 0.1575)

Figure 5. Reconstruction results. The thin solid lines represent the actual domains and the thick line represents the reconstructed ellipse.

where $\hat{m}$ and $\hat{M}$ are the elastic moment tensors while m and M are those in the rotated coordinate system by an angle θ.

Both reconstruction algorithms may use the linear or the quadratic method to find the center of a disc or an ellipse [19]. In this example, we use $U^{\text{quad}}(x) = \left(2x_1x_2, x_1^2 - x_2^2\right)$ to compute the location z using the following relations:

$$\sum_{i,j=1}^{2} M_{pq}^{ij}\left(\partial_i U_j^{\text{quad}}\right)(z) = 2\pi T^{-1}(t H_k[\mathbf{g}](te_l))_{pq} \tag{4.3}$$

as $t \to \infty$ where

$$T(a_{pq}) := \frac{1}{2}\sum_{p,q=1}^{2}(e_{klpq} + e_{klqp})a_{pq}, \qquad e_{klpq} := 2\pi t\ \partial^p \Gamma_{kq}(te^l).$$

It is worth mentioning that the numerical computation of $t H_k[\mathbf{g}](te_l)$ as $t \to \infty$ is done by a semi-analytic method, so there is no numerical truncation error in the limiting process.

Figure 5 shows the reconstructed ellipses as the number and the shape of inclusions varies. The background Lamé constants (λ, μ), the constants of inclusions $(\lambda_s, \mu_s) = (\tilde{\lambda}, \tilde{\mu})$ and the total size of the inclusions are given in the table. The areas of reconstructed disc and ellipse are also summarized along with the reconstructed center (x_c, y_c) by the quadratic method.

We further investigate the behavior of the ellipse reconstruction algorithm using 1, 3, 5 and 7 identical ellipses whose centers are shifted along a straight line. Figure 6 shows the placements of the ellipses and the reconstructed ellipse. The Lamé parameters of the inclusions are $(\tilde{\lambda}, \tilde{\mu}) = (9, 6)$ while those of the background are $(\lambda, \mu) = (6, 4)$. The size of a 45° slanted ellipse is two axis length times π, $ab\pi = 0.2 \times 0.05\pi$ and the center of the nth ellipse is $(0.6 - 0.1n, -0.6 + 0.1n)$. The computational results show that the area of the reconstructed ellipse is the sum of all inclusions and the reconstructed center is the geometric mean value of the inclusions as expected. One less expected observation is that the rotation angle θ_{ellipse} remains almost constant even when placement of the seven inclusions seems to be stretched along the upper-left to lower-right direction.

Example 5 (reconstruction of inclusions with the variable Lamé parameters)**.** In this example, we repeat the disc and the ellipse reconstruction algorithms described in example 4. However, all of inclusions have different Lamé parameters unlike the previous experiments. We randomly choose three to five ellipses among the ellipses shown in figure 3 for each of 50 experiments to make the computational domains D^p, $p = 1, \ldots, 50$. We assign different random values

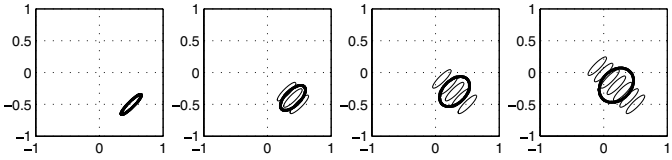

Number	(x_c, y_c)	(a, b) : $\frac{1}{\pi}\lvert D_{ellipse}\rvert$	$\theta_{ellipse}$
1	(0.49938, -0.50226)	(0.21913, 0.04565) : 0.01000	44.843
3	(0.39955, -0.39884)	(0.25102, 0.11977) : 0.03007	44.887
5	(0.29926, -0.29925)	(0.27784, 0.18069) : 0.05020	44.964
7	(0.19909, -0.19925)	(0.30356, 0.23182) : 0.07037	44.956

Figure 6. Reconstructed ellipses for the domains with 1, 3, 5 and 7 identical inclusions.

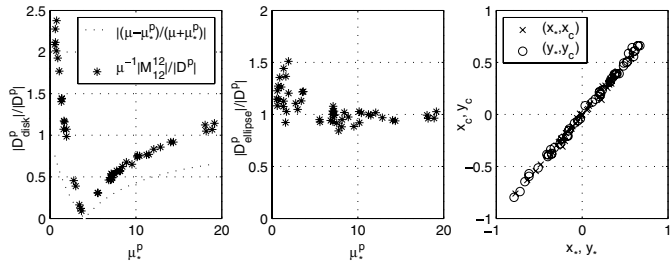

Figure 7. The leftmost and middle plots show the relative areas of reconstructed disc and ellipse as a function of the effective Lamé parameter μ_*. The rightmost plot presents the relation between the computed center (x_c, y_c) and the effective center (x_*, y_*) of the domain D^p

$\lambda_s < \lambda, \mu_s < \mu$ for the Lamé constants of $D_s \subset D^p$ in the first 20 experiments and randomly select $\lambda_s > \lambda, \mu_s > \mu$ for $D_s \subset D^p$, $p = 21, \ldots, 50$. Figure 7 shows the results of reconstructed area by the disc algorithm, by the ellipse algorithm, and the computed centers (x_c, y_c) by the quadratic method defined in (4.3).

The leftmost plot in figure 7 gives the reconstructed area relative to the inclusion size, $\left|D^p_{\text{disc}}\right| / |D^p| = \frac{1}{\mu}\left|M^{12}_{12}\right| / |D^p|$ of the disc reconstruction algorithm which does not require any information on the Lamé constants of the inclusions. The result has been plotted as a function of the effective Lamé constant μ^p_* defined by

$$\frac{\mu - \mu^p_*}{\mu + \mu^p_*} \sum_{D_s \subset D^p} |D_s| = \sum_{D_s \subset D^p} \frac{\mu - \mu^p_s}{\mu + \mu^p_s} |D_s|. \tag{4.4}$$

We noted that the result is almost identical to the result in figure 3 and it is a strong evidence that the total inclusion size can be easily estimated using the component M^{12}_{12} of the EMT and the effective Lamé constant μ_* defined in (4.4).

The rightmost figure shows the computed center (x_c, y_c) by the quadratic method which also does not require the Lamé parameters of the inclusions. This experiment shows that the computed inclusion center is almost identical to the effective center (x^p_*, y^p_*) of the inclusions D^p defined as follows:

$$x^p_* \sum_{D_s \subset D^p} \frac{\mu - \mu^p_s}{\mu + \mu^p_s} |D_s| = \sum_{D_s \subset D^p} x_s \frac{\mu - \mu^p_s}{\mu + \mu^p_s} |D_s|,$$

$$y^p_* \sum_{D_s \subset D^p} \frac{\mu - \mu^p_s}{\mu + \mu^p_s} |D_s| = \sum_{D_s \subset D^p} y_s \frac{\mu - \mu^p_s}{\mu + \mu^p_s} |D_s|,$$

where (x_s, y_s) is the center of the ellipse D_s. If we define 'μ-area' of an inclusion D_s as $\frac{\mu-\mu_s^p}{\mu+\mu_s^p}|D_s|$, then the effective center of inclusions is the geometric mean value of the centers of inclusions weighted by μ-area and the effective Lamé constant μ_*^p is nothing but the μ-area weighted mean value of μ_s.

The ellipse reconstruction algorithm requires a Lamé constant $(\tilde{\lambda}, \tilde{\mu})$ for the reconstructing ellipse. Although the selection of $\tilde{\mu}$ is more critical than $\tilde{\lambda}$, the change on the value of $\tilde{\lambda}^p$ makes easily $\pm 20\%$ changes of reconstructed area. It is natural to choose the effective μ_*^p for $\tilde{\mu}^p$ but the choice of $\tilde{\lambda}^p$ is not clear. The middle figure shows the area of the computed ellipse relative to the size of inclusions, $\left|D^p_{\text{ellipse}}\right| / |D^p|$ when $\tilde{\lambda}^p$ is set to be the area-weighted mean value of λ_s, $\tilde{\lambda}^p|D^p| = \sum_{D_s \subset D^p} \lambda_s |D_s|$. We have tried several other choices for $\tilde{\lambda}^p$ such as μ-area weighted λ_s; however, none of our choices is a clear winner compared to others. Further theoretical research regarding the EMT dependence on λ would give a better understanding on the ellipse reconstruction algorithm.

Acknowledgments

HK is partially supported by the grant KOSEF R01-2006-000-10002-0. EK is supported by BK21 Math. division at Seoul National University.

References

[1] Alessandrini G, Bilotta A, Formica G, Morassi A, Rosset E and Turco E 2005 Numerical size estimates of inclusions in elastic bodies *Inverse Problems* **21** 133–51
[2] Alessandrini G, Morassi A and Rosset E 2002 Detecting an inclusion in an elastic body by boundary measurements *SIAM J. Math. Anal.* **33** 1247–68
[3] Alessandrini G and Rosset E 1998 The inverse conductivity problem with one measurement: bounds on the size of the unknown object *SIAM J. Appl. Math.* **58** 1060–71
[4] Alessandrini G, Rosset E and Seo J-K 2000 Optimal size estimates for the inverse conductivity problem with one measurement *Proc. Am. Math. Soc.* **128** 53–64
[5] Ammari H and Kang H 2004 *Reconstruction of Small Inhomogeneities from Boundary Measurements* (*Lecture Notes in Mathematics* vol 1846) (Berlin: Springer)
[6] Ammari H and Kang H 2007 *Polarization and Moment Tensors with Applications to Inverse Problems and Effective Medium Theory* (*Applied Mathematical Sciences Series* vol 162) (Berlin: Springer)
[7] Ammari H, Kang H, Kim E and Lim M 2005 Reconstruction of closely spaced small inclusions *SIAM J. Numer. Anal.* **42** 2408–28
[8] Ammari H, Kang H, Nakamura G and Tanuma K 2002 Complete asymptotic expansions of solutions of the system of elastostatics in the presence of an inclusion of small diameter and detection of an inclusion *J. Elast.* **67** 97–129
[9] Arnold D N and Cheng R S 1988 The delta-trigonometric method using the single-layer potential representation *J. Integr. Equ.* **1** 517–47
[10] Beretta E and Francini E 2006 An asymptotic formula for the displacement field in the presence of thin elastic inhomogeneities *SIAM J. Math. Anal.* **38** 1249–61
[11] Brühl M, Hanke M and Vogelius M S 2003 A direct impedance tomography algorithm for locating small inhomogeneities *Numer. Math.* **93** 635–54
[12] Capdeboscq Y and Vogelius M S 2003 A general representation formula for the boundary voltage perturbations caused by internal conductivity inhomogeneities of low volume fraction *Math. Modelling Numer. Anal.* **37** 159–73
[13] Cedio-Fengya D J, Moskow S and Vogelius M 1998 Identification of conductivity imperpections of small diameter by boundary measurements: continuous dependence and computational reconstruction *Inverse Problems* **14** 553–95
[14] El Badia A and Ha-Duong T 2000 An inverse source problem in potential analysis *Inverse Problems* **16** 651–63
[15] Escauriaza L and Seo J-K 1993 Regularity properties of solutions to transmission problems *Trans. Am. Math. Soc.* **338** 405–30

[16] Friedman A and Vogelius M 1989 Identification of small inhomogeneities of extreme conductivity by boundary measurements: a theorem on continuous dependence *Arch. Ration. Mech. Anal.* **105** 299–326
[17] Han J 2003 Properties of electric and elastic polarization tensors *PhD Thesis* Seoul National University
[18] Kang H, Kim E and Kim K 2003 Anisotropic polarization tensors and detection of an anisotropic inclusion *SIAM J. Appl. Math.* **63** 1276–91
[19] Kang H, Kim E and Lee J-Y 2003 Identification of elastic inclusions and elastic moment tensors by boundary measurements *Inverse Problems* **19** 703–24
[20] Kang H and Lee H 2004 Identification of simple poles via boundary measurements and an application to EIT *Inverse Problems* **20** 1853–63
[21] Morassi A and Rosset E 2003 Detecting rigid inclusions, or cavities, in an elastic body *J. Elast.* **73** 101–26